

Evidence for a source size of less than 2000 AU in Quasar 2237+0305

Atsunori Yonehara^{1,2,3}

ABSTRACT

Recently, OGLE team have reported clear quasar microlensing signal in Q2237+0305. We have analyzed the microlens event of “image C” by using their finely and densely sampled lightcurves. From lightcurve fitting, we can unambiguously set the source size of $\lesssim 0.98$ Einstein Ring radius as a conservative limit. This limit corresponds to 2000(AU), if we adopt $M_{\text{lens}} \sim 0.1M_{\odot}$ obtained by a recent statistical study of mean mass of lens object. This gives a clear evidence for the existence of an accretion disk in the central region of the quasar.

Subject headings: accretion, accretion disks — galaxies: active — gravitational lensing — quasars: individuals (Q2237+0305)

1. INTRODUCTION

It is widely believed that central origins driving activity of quasars and AGNs (Active Galactic Nuclei) is an accretion disk surrounding a $10^{6\sim 9}M_{\odot}$ SMBH (supermassive black hole). To find a direct evidence for this general belief is one of the most exciting subjects in the current research in astronomy and astrophysics, but unfortunately, the expected angular size of accretion disks is too small ($\lesssim 1 \mu\text{as}$) to directly resolve spatially by using present observational instruments. For this reason, a proof of SMBH hypothesis remains as an unsolved problem in fields of quasar/AGN. Such a situation will not alter in near future.

¹Department of Astronomy, Kyoto University, Sakyo-ku, Kyoto 606-8502, Japan

²e-mail: yonehara@kusastro.kyoto-u.ac.jp

³Research Fellow of the Japan Society for the Promotion of Science

However, there is a strong tool to make it possible. That is so-called “quasar microlensing”. Following the first report of a detection of quasar microlensing in Q2237+0305 (“Einstein Cross” or “Huchra’s lens”) by Irwin et al. (1989) and subsequent extensive theoretical works (e.g., Wambsganss 1990), many researchers focused on this interesting subject and presented many meaningful results.

Roughly speaking, there are two different approaches to probe a structure of the central region of quasars. One is statistical approach by using long term monitoring data (e.g., Østensen et al. 1996) that are expected to contain many microlens events. Recently, Wyithe et al. have performed thorough statistical study; they compare real and mock observational results, and constrain transverse velocities of lens, the mean mass of the lens, source size, and so on (Wyithe, Webster, & Turner 1999, 2000b, 2000c). Another is to focus on a single HME (High Magnification Event), on the basis of reasonable assumptions and/or some statistical features, and constrain a source size or structure (e.g., Wyithe et al. 2000a, and references therein).

In this *letter*, thus we take the latter approach and performed lightcurve fitting for the accurately and densely observed microlensing event that OGLE team have detected in Q2237+0305 lately (Wozniak et al. 2000a, 2000b), to put a limit on the microlensed source size. In section 2, we briefly present our method to fit an observed lightcurve and the results and discussions are shown in section 3.

2. LIGHTCURVE FITTING

The *V*-band monitoring data of OGLE team show that there is a dramatic brightening in image A and abrupt brightening and subsequent decay in image C ($> 0.5\text{mag}$), whereas flux changes have been less significant in images B and D (they have only $\sim 20\%$ flux variation) compared with image A and C. This suggest that microlens events have occurred in images A and C independently. While the behavior of image A was complicated and could be caused by complicated (many) caustics, that of image C seems to be quite simple and can be understood in terms of a single-caustic induced HME. Therefore, applying approximate magnification formulae which are appropriate in the vicinity of a caustic, we try to fit the lightcurve of image C. Concrete formulae of magnification (μ) for a source position (x, y) are shown in Fluke & Webster (1999) for “fold caustic (hereafter, FC)” case and Zakharov (1995) for “cusp caustic (hereafter, CC)” case.

To characterize properties of caustics, e.g., curvature of fold caustic, we should evaluate derivatives of Fermat potential (ϕ) for gravitational lensing phenomena. In quasar

microlensing cases, Fermat potential is written as follows,

$$\begin{aligned} \phi = & \frac{1}{2}\{(\eta - x)^2 + (\xi - y)^2 - \kappa_c(\eta^2 + \xi^2) - \gamma [(\eta^2 - \xi^2) \cos 2\theta + 2\eta\xi \sin 2\theta]\} \\ & - \sum_{i=1}^{N_{\text{lens}}} \log\{\epsilon_i [(\eta - \eta_i)^2 + (\xi - \xi_i)^2]^{1/2}\}, \end{aligned} \quad (1)$$

where, (η, ξ) is an image position, γ and θ is shear and its direction, κ_c is convergence arising due to continuous (smooth) mass distribution, (η_i, ξ_i) and ϵ_i in this equation represent the i -th lens position and its normalized mass, and N_{lens} is the total number of compact, stellar lens. Here, κ_c plus contributions of compact, stellar lens should be almost equal to total convergence (κ) that is determined by macrolens model. All the length scales are normalized by the Einstein-ring radius (r_E).

Unfortunately, we are not able to know complete spatial distribution and mass of compact, stellar lens objects, and it is impossible to characterize exact properties of caustics. Therefore, in this study, we assume that only one single lens object plays a significant role in the HME and contributions from other lens objects are negligible ($N_{\text{lens}} = 1$), i.e., we only consider about so-called ‘‘Chang-Refsdal lens (Chang & Refsdal 1984)’’ situation (single lens object plus external convergence and shear), for simplicity, and characterize the properties. Applied values of convergence and shear is one of the best fit value on image C for macrolens model of Q2237+0305, $\kappa = 0.69$ and $\gamma = 0.71$ (Schmidt, Webster & Lewis, 1998). In some complicated case (e.g., lens objects are clustering), situation may be modified, or in the worst case, above assumption will break down. However, if this assumption holds (e.g., $\kappa_c \sim \kappa$ is the case), we are able to characterize the feature of FC and CC by only one parameter (θ).

In the case of the Chang-Refsdal lens, 2 different types of cusp caustic will be formed at 4 or 6 angular positions of the closed caustic curve (see Chang & Refsdal 1984), and the fold caustics appear as connecting these cusp caustics. Thus, we consider 2 cusp cases and 4 representative fold cases for an angle range of $\theta = 0 \sim \pi/2$ because of its symmetry. Moreover, we only consider about circular-shape source with top-hat brightness profile, i.e., neglect the effect of inclination angle, brightness profile. Therefore, magnification (\mathcal{M}) at any given source position (x, y) is obtained by the integration of μ on the circular disk with radius R . Assuming top-hat brightness profile is fairly simple treatment because the shape of microlensing lightcurve depends on source brightness profile (e.g., Yonehara et al. 1999). However, the resultant source size can be regarded as an effective (equivalent) source size and we use the top-hat brightness profile for convenience to numerical integrations (with 1000 mesh number in this study).

To include magnification caused by macrolensing and another caustics for microlensing,

here, we add constant magnification, M_0 , plus gradual change of the magnification, $\dot{M}_0 \cdot t$, to the total magnification. The latter mimics magnification changes for the ensemble of other microlens and this gradual change make the fits better (Wyithe and Turner, private communication). Furthermore, intrinsic variability of this quasar may be long duration with small amplitude (Wyithe et al. 2000d), and this term may also mimic the intrinsic variabilities of quasar.

Additionally, we should evaluate the apparent magnitude of quasar without any microlensing and macrolensing, i.e., the intrinsic magnitude, m_0 . It is quite difficult because quasars have intrinsic variabilities and also the observed magnitude of Q2237+0305 is affected by small amplitude and/or long timescale microlensing. Fortunately, from the monitoring data by Østensen et al.(1996) and the OGLE team, the observed magnitude of image C is roughly constant at ~ 18.6 mag long before the recent HME. We thus take this as the magnitude of this quasar without any microlensing. Moreover, by using the previously applied value of κ and γ , we can evaluate the macrolens magnification of image C, and the intrinsic magnitude is estimated to be $m_0 = 18.6 - 2.5 \log [(1 - \kappa)^2 - \gamma^2] \sim 19.6$.

Finally, assuming the source trajectory is straight and determine source velocity on the source plane, $\vec{v} = (v_x, v_y)$, time when the source crosses a caustic (FC case) or x -axis (CC case), T_0 , the expected microlensing lightcurve for any given parameter is obtained from $m(t) = m_0 - 2.5 \log [M_0 + \dot{M}_0 \cdot t + \mathcal{M}(t)]$ (for CC case and fold caustic grazing case, impact parameter, d is also required).

To obtain the best fit lightcurve and its parameter, we minimize χ^2 value between the observed lightcurve, $m_{\text{obs}}(t)$, and the mock lightcurve for a given parameter, $m(t)$, for each caustic case (FC and CC) by using one of downhill simplex method, so-called “AMOEBa” routine (Press et al. 1986). Nonetheless, caustic is a kind of singularities, and fitting methods including singularities do not work so well. For this reason, we subdivide each caustic case into all considerable path cases (depicted in figure 1) and perform lightcurve fitting at every possible case. After the best fit parameters are obtained, we compare reduce χ^2 for all the possible cases for each of FC and CC, and determine the best fit (smallest χ^2) parameters for each FC and CC case.

In this lightcurve fitting, we only took into account data points around the peak of image C ($JD - 2450000 = 1289.905 \sim 1529.531$, total number of used data points is 83). Of course, we can also taken into account data points before and after the peak, but in those epochs, distance between the source and caustic could be larger than that in the peak region. Thus, it is not clear whether the approximation for magnification is reasonable or not before and after the peak. And so, we have restricted data points only around the peak.

3. RESULTS AND DISCUSSIONS

Our resultant, best fit parameters for all the cases that we have considered are summarized in table 1. Some resultant path of source, the best fit lightcurve, source size dependence of reduced χ^2 are also shown in figures 2 and 3 (degree of freedom is $83 - 5 = 78$ for FC, $83 - 6 = 77$ for CC). In the case of a infinitely-small size source, expected lightcurves for microlens event are quite different from case to case, i.e., a lightcurve for FC case and that of CC case is clearly different, and also, difference between that of fold-1 and fold-2 (figure 1) is evident and so on. But, as you can easily see in these table and figures, the fitting for all cases works well (the best-fit reduced χ^2 is ~ 1). This fact owing to the finite-size source effect, and we can manage to reproduce the observed feature at every considerable case.

We also performed a Monte-Carlo simulation for every case to estimate confidence region of best fit parameter by using following procedures; (1) Supposing that the best fit parameter is real parameter, we calculate an ideal lightcurve without any errors, (2) Add random errors with the magnitude corresponding to the observational error dispersion, and sample this lightcurve at the times corresponding to the actually observed times, we obtain a mock lightcurve. (3) By using this mock lightcurve, we perform a lightcurve fitting again for all considerable cases (at FC and CC case indicated before, see also fig 1) and obtain a set of the best fit parameters for the mock lightcurve.

Iterating procedure (2) and (3) for 100 times in this study, summarizing the best fit values for mock lightcurves, and we can evaluate a confidence region. To evaluate the 90% confidence region from Monte-Carlo results, we calculate total χ^2 between lightcurve which is actually observed and that is obtained from the parameters of Monte-Carlo result. Subsequently, we pick up 90% parameter sets which have smaller total χ^2 . From these selected parameter sets, finally, we can obtain maximum and minimum values of parameters and we define ranges between these maximum and minimum as the 90% confidence region.

In figures 2 and 3, we also presented a histogram for the χ^2 differences between “mock” lightcurves and the best fit lightcurve, and ideal χ^2 distribution curves for corresponding degrees of freedom (5 for FC, 6 for CC). These two exhibit similar distributions and our confidence region estimate seems to be reasonable.

For every case, if the source size is larger than the best fit value, expected magnification will be suppressed, lightcurve will become shallow, and goodness of fit is reduced. On the other hands, if the source is smaller than the best fit value, expected magnification will be enhanced, lightcurve will become sharp, and goodness of fit reduced, too. These are qualitative reason why the source size is limited in somewhat small range.

Considering all our fitting result, at least, we can say that the source size of Q2237+0305 should be smaller than ~ 0.98 Einstein-ring radius (more than 90% confidence level). This upper limit is given in the case of FC (fold 3 in table 1), while another case suggests a much smaller source size. Thus, this limit is a fairly conservative upper limit for the source. Since the Einstein-ring radius of quasar microlensing is typically $\lesssim 1 \mu\text{as}$, our result indicates the existence of a sub- μas source in quasar !

To obtain the actual size, we have to calculate r_E for relevant parameters. If we assume $1.0M_\odot$ as a mass of lens object (M_{lens}) and the Hubble constant $H_0 = 67\text{km s}^{-1} \text{Mpc}^{-1}$ (Kundić et al. 1997), r_E will be corresponds to 10^{17}cm . This value strongly depends on H_0 ($r_E \propto H_0^{-1/2}$) and the lens mass ($r_E \propto M_{\text{lens}}^{1/2}$) rather than the cosmological parameters in this case ($\sim 10\%$ uncertainty covers roughly all the reasonable range). And finally, we get $10^{17}\text{cm} \sim 7 \times 10^3\text{AU}$ as the resultant upper limit to the source size. This value is consistent with the result of the statistical research performed by Wyithe et al. (2000c). Moreover, for the $\sim 0.1M_\odot$ lens object case suggested by Wyithe et al. (2000b) as a mean lens mass, the size will be reduced by some factor and become $\sim 2 \times 10^3\text{AU}$!. Alternatively, the lens object may be a stellar object, and so, there is an upper mass limit to exist stably. Even if we adopt this upper limit $\sim 100M_\odot$ for the lens mass, the size will be $\sim 0.3\text{pc}$, at most. Therefore, our result strongly supports the existence of an accretion disk in a quasar and that the accretion disk smaller than this size is a fairly dominant source of radiation from the quasar, at least in the V -band at observer frame. Additionally, resultant effective transverse velocity on the source plane is $\lesssim 10^5(\text{km s}^{-1})$, and is also consistent to the value presented by Wyithe, Webster & Turner, 1999.

On the other hands, if we assume that the accretion disk is a type described by the standard accretion disk model (Shakura & Sunyaev 1973), we can also estimate the effective source size from its luminosity. The magnitude of this quasar in the absence of a macrolens effect is easily converted into flux, f_ν (Wozniak et al. 2000a). If we denote the absorption as A_V mag and adopt the luminosity distance (d_L) to the quasar, luminosity of the quasar at this observed waveband (L) will estimated to be $L \sim \nu(f_\nu \cdot 10^{0.4A_V})4\pi d_L^2 \sim 3.7 \times 10^{42+0.4A_V} \text{erg s}^{-1}$. Furthermore, radiation process of the standard accretion disk is blackbody radiation, and the effective temperature (T_{eff}) of the accretion disk at this waveband corresponds to $\sim 2.5 \times 10^4 \text{K}$. On the other hands, we can relate the effective temperature, luminosity and the radius through the central black hole mass and accretion rate,

$$T_{\text{eff}} \sim \left(\frac{3}{4\pi\sigma} \right)^{1/4} L^{1/4} r^{-1/2}, \quad (2)$$

where, σ is the Thomson-scattering cross section. Consequently, we are able to estimate the effective source size being $r \sim 2.0 \times 10^{14+0.2A_V} \text{cm}$. There is an uncertainty in A_V , but this

is consistent with our results and strongly indicates the existence of an accretion disk. We should pay attention that we do not insist the existing source should be a standard-type accretion disk (other accretion disk models may be also consistent with our results). Rauch & Blandford (1991) reported that the accretion disk in Q2237+0305 is non-thermal or optically thin. But, there are some ambiguities in this work (e.g., absorption, lens mass), and it is quite difficult to support or oppose the report from our results. To specify disk models, we have to do more extensive monitorings and/or analyze multi-band microlens lightcurves to compare the resultant source sizes.

The performed fitting procedure do work, but strictly speaking, all our best-fit reduced χ^2 are somewhat larger than 1. This means the goodness of fit of our results is not extremely good and probably, there may be some systematic errors that we do not take into account. In this work, we neglect the detailed feature about source, magnification patterns and intrinsic variabilities of the quasar. However, if such effects are really existing, the shape of the lightcurve will be systematically altered and the best-fit reduced χ^2 may be increased by these effects. There are difficulties to be take into account all above possibilities in our procedure, but it will be done in future.

In future work, we should further develop quasar microlens technique in two statistical ways. One is to study statistical properties of magnification near FC and CC. Although the statistical features have already been studied by many researchers (e.g., Wambsganss & Kundić 1995), the effect, such as, lens object clustering that affect properties of magnification in the vicinity of caustic is not well understood. The other is to continue monitoring this kind of quasars, sample similar microlensing events more and more. Such analysis may be able to reduce ambiguities arising due to unknown lens mass, and/or different features of caustic networks and so on.

The author would like to express his thanks to S. Mineshige for his extensive supports, E.L. Turner, J.S.B. Wyithe, K. Ioka, K. Mitsuda, K. Yoshikawa, T. Takeuchi, M. Umemura, A. Burkert and Y. Suto for their helpful comments, and anonymous referee for his/her valuable suggestions and comments. The author also acknowledge the OGLE team for making their monitoring data publically available. This work was supported in part by the Japan Society for the Promotion of Science (9852).

REFERENCES

Chang, K., & Refsdal, S., 1984, A&A, 132, 168

- Fluke, C.J., & Webster, R.L., 1999, MNRAS, 302, 68
- Irwin, M.J., Webster, R.L., Hewitt, P.C., Corrigan, R.T., & Jedrzejewski, R.I. 1989, AJ, 98, 1989
- Kundić T., et al. 1997, ApJ, 482, 75
- Østensen, R., et al. 1996, A&A, 309, 59
- Press, W.H., Flannery, B.P., Teukolsky, S.A., & Vetterling, W.T. 1992, “Numerical Recipes” (2nd ed.; Cambridge: Cambridge Univ. Press)
- Rauch, K.P., & Blandford, R.D. 1991, ApJ, 381, L39
- Schmidt, R., Webster, R.L., & Lewis, G.F., 1998, MNRAS, 295, 488
- Shakura, N.I., & Sunyaev, R.A. 1973, A&A, 24, 337
- Wambsganss, J. 1990, “Gravitational Microlensing”, Dissertation der Fakultät für Physik der Ludwig-Maximilians-Universität, München
- Wambsganss, J., & Kundić, T. 1995, ApJ, 450, 19
- Wozniak, P.R., Alard, C., Udalski, A., Szymanski, M., Kubiak, M., Pietrzynski, G., & Zebrun, K. 2000a, ApJ, 529, 88
- Wozniak, P.R., Udalski, A., Szymanski, M., Kubiak, M., Pietrzynski, G., Soszynski, I., & Zebrun, K. 2000b, ApJ, 540, L65
- Wyithe, J.S.B., Webster, R.L., & Turner E.L. 1999, MNRAS, 309, 261
- Wyithe, J.S.B., Webster, R.L., Turner, E.L., & Mortlock, D.J. 2000a, MNRAS, 315, 62
- Wyithe, J.S.B., Webster, R.L., & Turner E.L. 2000b, MNRAS, 315, 51
- Wyithe, J.S.B., Webster, R.L., & Turner E.L. 2000c, MNRAS, 318, 762
- Wyithe, J.S.B., Webster, R.L., Turner, E.L., & Agol, E. 2000d, accepted to MNRAS (astro-ph/0001306)
- Yonehara, A., Mineshige, S., Fukue, J., Umemura, M., & Turner, E.L. 1999 A&A, 343, 41
- Zakharov, A.F. 1995, A&A, 293, 1

	fold-1	fold-2	fold-3	fold-4	cusp-1	cusp-2
angle	0.00	0.50	1.00	1.50	0.32	1.57
best fit	FC1	FC1	FC2	FC1	CC2	CC2
$R(10^{-1})$	$1.78_{-0.18}^{+0.19}$	$2.42_{-0.22}^{+0.23}$	$8.50_{-3.73}^{+1.32}$	$7.64_{-0.72}^{+0.86}$	$2.14_{-0.54}^{+1.36}$	$1.00_{-0.24}^{+0.80}$
$v_x(10^{-2})$	$0.30_{-0.06}^{+0.06}$	$0.42_{-0.08}^{+0.08}$	0	$1.31_{-0.25}^{+0.23}$	$-0.04_{-0.03}^{+1.79}$	$-0.02_{-0.02}^{+0.79}$
$v_y(10^{-2})$	$0.38_{-0.04}^{+0.04}$	$0.49_{-0.14}^{+0.07}$	$2.74_{-0.72}^{+0.73}$	$1.57_{-0.13}^{+0.17}$	$0.63_{-0.59}^{+0.10}$	$0.30_{-0.30}^{+0.04}$
T_0	1348_{-3}^{+3}	1351_{-4}^{+2}	1366_{-2}^{+2}	1350_{-4}^{+2}	1366_{-8}^{+348}	1366_{-8}^{+308}
$d(10^{-1})$	0	0	$6.38_{-0.84}^{+0.47}$	0	$3.24_{-6.58}^{+57.3}$	$1.10_{-2.33}^{+20.8}$
M_0	$9.05_{-2.89}^{+2.37}$	$9.23_{-2.27}^{+1.91}$	$18.55_{-1.58}^{+1.12}$	$9.03_{-2.31}^{+2.27}$	$20.06_{-5.83}^{+1.05}$	$20.02_{-6.46}^{+1.09}$
$M_0(10^{-3})$	$-3.05_{-1.59}^{+1.90}$	$-3.12_{-1.26}^{+1.49}$	$-8.82_{-0.68}^{+0.96}$	$-3.02_{-1.52}^{+1.52}$	$-9.88_{-0.18}^{+3.76}$	$-9.86_{-0.20}^{+4.18}$
$\bar{\chi}^2$	1.46	1.49	1.48	1.47	1.33	1.30

Table 1: Best fit parameters for several possible HME (see figure 1) and their reduced χ^2 ($\bar{\chi}^2$). All the length scales and time scale is normalized by r_E and one day. The unit of velocity is the Einstein-ring radius divided by a day. For T_0 , $T_0 = 0$ correspond to $JD - 2450000 = 0$. Upper and lower value denoted beside the best fit parameters show a 90% confidence level which calculated from Monte-Carlo simulation (see the text).

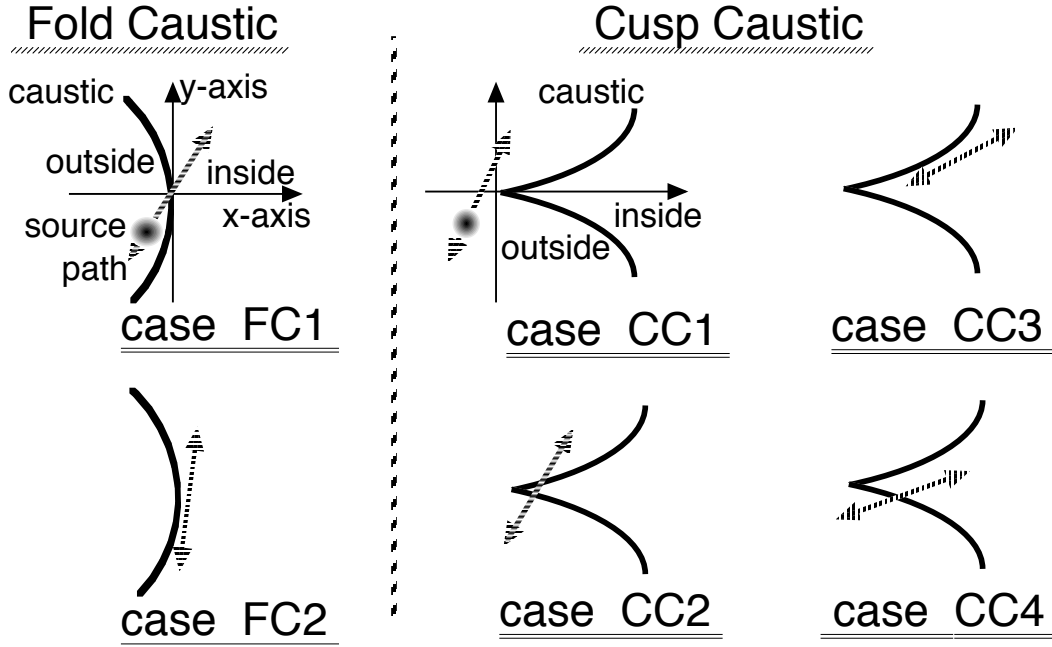


Fig. 1.— Schematic view of possible HME. All the six cases to reproduce the observed, fairly symmetric HME event are shown: 2 are fold caustic cases and 4 are cusp caustic.

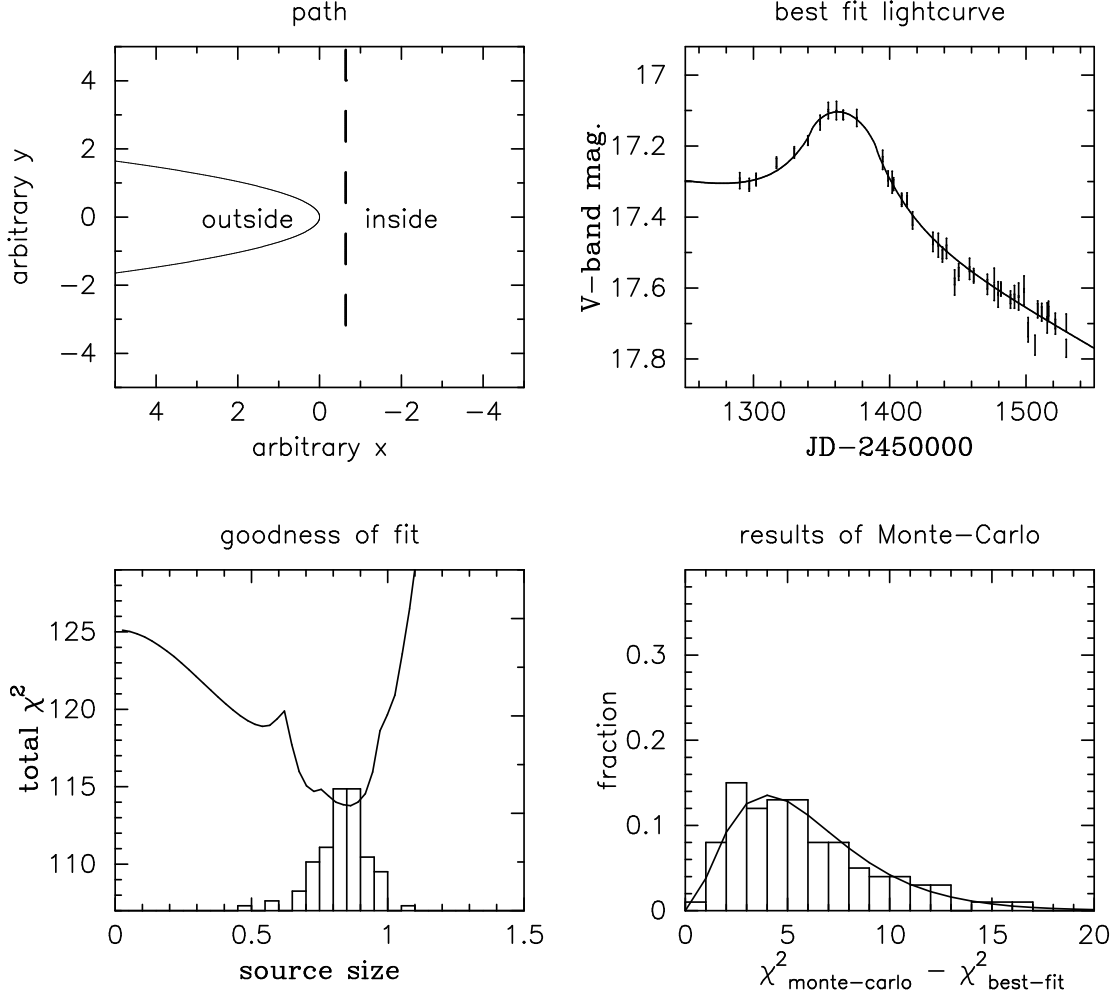


Fig. 2.— Fitting results in a case of fold caustic (fold-3). In upper left panel, the best fit source path (dashed line) and relative to caustic (bold line) is depicted. Upper right panel is observed flux (error bar) and the best fit lightcurve (bold line). Lower left panel is total χ^2 value respect to source size (bold line), and result of Monte-Carlo simulation (histogram). Lower right panel distribution of χ^2 with 5 degree of freedom (bold line) and distribution of χ^2 difference between mock lightcurve and the best fit lightcurve (histogram). All the length scale is r_E . Kinks in source size dependence of total χ^2 (lower left panel) are caused by changes from a best-fit subdivided case to another subdivided case, e.g., at source size ~ 0.6 , the best-fit, subdivided case changes from FC1 to FC2.

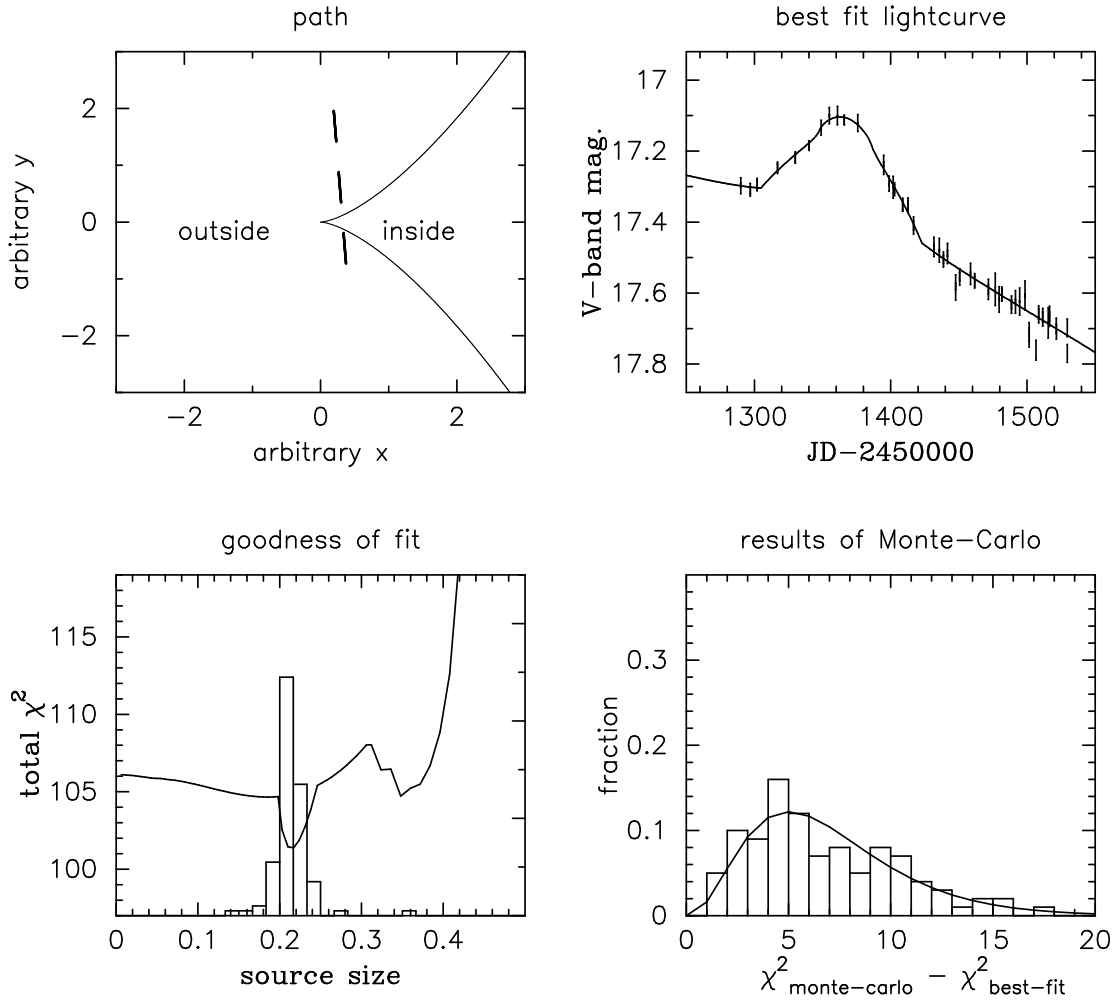


Fig. 3.— Same as figure 2 but cusp caustic case (cusp-1). Degree of freedom of lower right panel is 6 in this case. Kinks in source size dependence of total χ^2 value (lower left panel) appeared with the same reason as in figure 2